Advances in Nano Research, *Vol. 13, No. 1 (2022) 77-86*
https://doi.org/10.12989/anr.2022.13.1.077

Maxwell nanofluid flow through a heated vertical channel with peristalsis and magnetic field

Z. M. Gharsseldien*[2] and A.S. Awaad[1,3a]

[1]*Department of Mathematics, College of Arts and Science, Prince Sattam Bin Abdul-Aziz University, 054-11991 Wadi Adwassir, Riyadh, Saudi Arabia*
[2]*Department of Mathematics, Faculty of Science (Men), Al-Azhar University, Nasr City,11884, Cairo, Egypt*
[3]*Department of Mathematics, Faculty of Science (Girls), Al-Azhar University, Nasr City,11754, Cairo, Egypt*

(*Received April 25, 2021, Revised November 18, 2021, Accepted May 15, 2022*)

Abstract. This paper studied the peristaltic transport of upper convected Maxwell nanofluid through a porous medium in a heated (isothermal) symmetric vertical channel. The nanofluid is assumed to be electrically conducting in the presence of a uniform magnetic field. These phenomena are modeled mathematically by a differential equations system by taking low Reynolds number and long-wavelength approximation, the yield differential equations have solved analytically. A suggested new technique to display and discuss the trapping phenomenon is presented. We discussed and analyzed the pumping characteristics, heat function, flow velocity and trapping phenomena which were illustrated graphically through a set of figures for various values of parameters of the problem. The numerical results show that, there are remarkable effects on the vertical velocity, pressure gradient and trapping phenomena with the thermal change of the walls.
Keywords: heated channel; magnetic field; peristalsis; upper-convected maxwell nanofluid

1. Introduction

A key parameter to study nanofluids' applicability for heat transfer enhancement of flowing liquids is their thermal conductivity. Water, engine oil, monoethylene glycol and ethylene glycol, which are the most widely used fluids in different applications, are called conventional heat transfer fluids. These fluids have relatively low thermal conductivity than nanofluids' thermal conductivity and convective heat transfer coefficient Chen *et al.* (2014).

Nanofluids are prepared by dispersing nanometer-sized materials (nanoparticles, nanofibers, nanotubes, nanowires, nanorods, nanosheets, or droplets) in base fluids. The shape geometry of nanoparticles and their effect was studied in some research papers as Akbar *et al.* (2017). Hamilton and Crosser (1962) suggested that a nanofluid thermal conductivity depends on nanoparticle shape sphericity. Sphericity is defined as the ratio of a sphere's surface area, with a volume equal to that of the particle, to the particle's surface area. The particle with a perfectly spherical shape has a maximum value of sphericity which equal 1 Sheikholeslami and Ganji (2017). Based on some experiments, Timofeeva *et al.* (2009) introduced a new form of some thermophysical properties depends on nanoparticle shape. Based on nano-materials characteristics e.g., large surface areas, size, shape and dimensions etc. Amin and Alazba (2014) presented an overview the availability and practice of different nanomaterials based membranes for removal of bacteria and viruses, organic compounds and inorganic solutes etc. present in polluted waters.

Nanofluids are used in the thermosyphons, heat exchangers, solar energy and absorption refrigeration systems (Sözen *et al.* 2014, Buschmann and Franzke 2014, Mohamad *et al.* 2013 and Chen *et al.* 2014). Nanoparticle diameter, nanoparticle volume fraction nanofluid temperature, nanoparticle thermal conductivity, base fluid thermal conductivity are the different parameters that can directly influence the nanofluid thermal conductivity.

In analytical conduction problems, two commonly used boundary conditions are isothermal and isoflux and these two are mutually exclusive. In an isothermal case, the surface holds a fixed temperature regardless of how much heat flow occurs because of that temperature. While in an isoflux case, a constant heat flux (in or out) is maintained at the surface regardless of how high (or low) the temperature gets because of that heat flux. (Cheng *et al.* 1990, Boulama and Galanis 2004) introduced some analytical, theoretical solutions of the fully developed mixed convection flow in a vertical channel under various fundamental thermal boundary conditions.

The buoyant force causes the fluid to rise when the density decreases due to an increase in temperature. The primary force that resists is the viscous force. The ratio of buoyant force to the viscous force acting on a fluid in the velocity boundary layer is called Grashofe number, which has a significant effect on the reversed fluid in the isothermal systems, as pointed out in Cheng *et al.* (1990). Shah *et al.* (2018) presented a systematic review of 30 articles and they studied the effects of mixed convection parameter and Grashof number on the flow of various fluids. The effects of bioconvection phenomenon, chemical

*Corresponding author, Ph.D.,
E-mail: gharsseldienz@gmail.com
[a]Ph.D., E-mail: a.asar@psau.edu.sa

ISSN: 2287-237X (Print), 2287-2388 (Online)

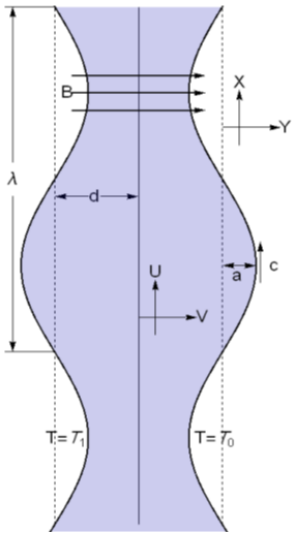

Fig. 1 Geometry of the problem

reaction and heat parameter in MHD boundary layer flow of a non-Newtonian nanofluid with Cattaneo-Christov heat flux past a stretchable cylinder is studied by Sharif *et al.* (2021).

No doubt the nanotechnology with peristalsis is hot topic of research at present, see (Abbasi *et al.* 2015, Akbar *et al.* 2012, Ghasemi *et al.* 2016, Hayat *et al.* 2016, 2017, Ibrahim *et al.* 2019, Mosayebidorcheh and Hatami 2018, Noreen 2018, Rachid 2015, Reddy and Makinde 2016, Sadaf *et al.* 2018, Sayed *et al.* 2016, Abd Elmaboud 2018, Elmaboud *et al.* 2019, Kot and Elmaboud 2021 and Vajravelu *et al.* 2011). In this article, we studied the peristaltic transport of nanofluid through a porous medium in a symmetric heated vertical channel, the effect of a magnetic field is taken into account. The pumping characteristics, heat function, flow velocity and trapping phenomena are analyzed for various parameter values of upper convected Maxwell fluid.

2. Problem formulation

Consider the peristaltic transport of a two-dimensional flow of an incompressible Maxwell nanofluid with MHD through a porous space in a vertical symmetric channel. The peristaltic waves are traveling along the X- axis with speed c. Taking the two-dimensional cartesian coordinates (Y, X) where X-axis is taken in motion direction (Vertical Axis) while Y-axis is normal to it (Horizontal Axis) as shown in Fig. (1).

The equations of the walls of a symmetric channel can be written as

$$Y = \pm H = \pm d \pm a\, sin\frac{2\pi}{\lambda}(X - c\ t) \tag{1}$$

where d is the mean half-width of the channel, a is the amplitudes of the waves, λ is the wavelength, c is the velocity of propagation and t is the time. Let (U, V) are the velocity components in X and Y directions, respectively. Considering $B = (0, B_0, 0)$ is the uniform magnetic field applied in the transverse direction to the flow, then the MHD force

$$J \times B = -\sigma_{nf} B_0^2 U$$

J is the total current density if there are no applied or polarized voltages and σ_{nf} is the nanofluid's electric conductivity. If R is Darcy's resistance for a fluid in a porous medium, wherein Maxwell fluid Darcy's resistance R satisfies the relation

$$\left(1 + \lambda_1 \frac{d}{dt}\right) R = -\frac{\mu_{nf}}{K} V,$$

where K is the permeability parameter and $\left(\frac{d}{dt}\right)$ is the material time derivative. Then equations of mass, momentum and temperatur (Sobamowo 2018, Vajravelu *et al.* 2011) which describe this motion will be in the form

$$\frac{\partial U}{\partial X} + \frac{\partial V}{\partial Y} = 0, \tag{2}$$

$$\begin{aligned} &\rho_{nf}\left(1 + \lambda_1 \frac{d}{d\ t}\right)\left(\frac{d\ U}{d\ t}\right) \\ &= \left(1 + \lambda_1 \frac{d}{d\ t}\right)\left[-\frac{\partial P}{\partial X} + \frac{\partial S_{XX}}{\partial X} + \frac{\partial S_{XY}}{\partial Y} - \sigma_{nf} B_0^2 U\right] \\ &+ \left(1 + \lambda_1 \frac{d}{d\ t}\right)\left[g\ (\rho\alpha)_{nf}(T - T_0)\right] - \frac{\mu_{nf}}{K} U, \end{aligned} \tag{3}$$

$$\begin{aligned} &\rho_{nf}\left(1 + \lambda_1 \frac{d}{d\ t}\right)\left(\frac{d\ V}{d\ t}\right) \\ &= -\left(1 + \lambda_1 \frac{d}{d\ t}\right)\left[\frac{\partial P}{\partial Y} + \frac{\partial S_{YX}}{\partial X} + \frac{\partial S_{YY}}{\partial Y}\right] - \frac{\mu_{nf}}{K} V, \end{aligned} \tag{4}$$

$$\begin{aligned} (\rho C)_{nf}\left(\frac{d\ T}{d\ t}\right) = k_{nf}\left(\frac{\partial^2 T}{\partial X^2} + \frac{\partial^2 T}{\partial Y^2}\right) + S_{XX}\frac{\partial U}{\partial X} + S_{XY}\frac{\partial U}{\partial Y} \\ + S_{YX}\frac{\partial V}{\partial X} + S_{YY}\frac{\partial V}{\partial Y}, \end{aligned} \tag{5}$$

$$S_{XX} + \lambda_1\left[\frac{dS_{XX}}{dt} - 2\left(S_{XX}\frac{\partial U}{\partial X} + S_{XY}\frac{\partial U}{\partial Y}\right)\right] = 2\mu_{nf}\frac{\partial U}{\partial X}, \tag{6}$$

$$\begin{aligned} S_{XY} or S_{YX} + \lambda_1\left[\frac{dS_{XY}}{dt} - S_{XX}\frac{\partial V}{\partial X} - S_{YY}\frac{\partial U}{\partial Y}\right] \\ = \mu_{nf}\left(\frac{\partial V}{\partial X} + \frac{\partial U}{\partial Y}\right), \end{aligned} \tag{7}$$

$$S_{YY} + \lambda_1\left[\frac{dS_{YY}}{dt} - 2\left(S_{XY}\frac{\partial V}{\partial X} + S_{YY}\frac{\partial V}{\partial Y}\right)\right] = 2\mu_{nf}\frac{\partial V}{\partial Y}, \tag{8}$$

where ρ_{nf} is the nanofluid density, P is the pressure, $(\rho C)_{nf}$ is the heat capacity of the nanofluid, T is temperature and k_{nf} is the thermal conductivity of the nanofluid. S is the extra stress tensor for Maxwell fluid, λ_1 is the fluid relaxation time, μ_{nf} is the kinematic viscosity coefficient of the nanofluid. g is the acceleration due to gravity and α_{nf} is the thermal expansion coefficient of nanofluid.

Introducing a wave frame (y, x) moving with the velocity c away from the laboratory frame (Y, X), by the transformations

$$x = X - c\ t, \quad y = Y, \quad u = U - c, \\ v = V, \quad p(x) = P(X,t), \tag{9}$$

where u and v are the fluid velocity components, p is pressure in the wave frame of references. Also, introducing the non-dimensional variables

$$\left.\begin{aligned} \bar{x} &= \frac{x}{\lambda}, \quad \bar{y} = \frac{y}{d}, \quad \bar{t} = \frac{ct}{\lambda}, \quad \bar{u} = \frac{u}{c}, \\ \bar{v} &= \frac{v}{\delta c}, \quad h = \frac{H}{d}, \quad \bar{\lambda}_1 = \lambda_1 \frac{c}{d}, \quad b = \frac{a}{d}, \\ \delta &= \frac{d}{\lambda}, \quad p = \frac{d^2\bar{p}}{\mu_f c\,\lambda}, \quad M = \sqrt{\frac{\sigma_f}{\mu_f}} B_0 d, \\ \bar{S} &= \frac{d}{c\ \mu_f} S, \quad R_e = \frac{\rho_f\ c\ d}{\mu_f}, \quad \bar{K} = \frac{K}{d^2}, \\ \Theta &= \frac{T - T_0}{T_1 - T_0}, \quad G_r = \frac{g\ (\rho\alpha)_f\ d^2(T_1 - T_0)}{c\ \mu_f}, \\ E_c &= \frac{c^2}{C_f(T_1 - T_0)}, \quad P_r = \frac{\mu_f\ C_f}{k_f} \end{aligned}\right\} \tag{10}$$

where M is Hartmann number, R_e is Reynolds number, Θ is the dimensionless temperature, C_f is the specific heat of the fluid, μ_f is the kinematic viscosity coefficient of the fluid, G_r is Grashof number , P_r is Prandtl number, E_c is Eckert number and b is the amplitude ratio. Then after using the transformations (9), dimensionless (10), dropping bars and under the assumptions of long-wavelength ($\delta \ll 1$) and low Reynolds number, Eqs. (2)-(8) become on the form.

$$\frac{\partial p}{\partial x} = \frac{\partial S_{xy}}{\partial y} - \left(\frac{\sigma_{nf}}{\sigma_f} M^2 + \frac{\mu_{nf}}{\mu_f}\frac{1}{K}\right)(u+1) + \frac{(\rho\alpha)_{nf}}{(\rho\alpha)_f}\ G_r\ \Theta, \tag{11}$$

$$\frac{\partial p}{\partial y} = 0, \tag{12}$$

$$\frac{1}{P_r}\frac{k_{nf}}{k_f}\frac{\partial^2\Theta}{\partial y^2} + E_c\ S_{xy}\frac{\partial u}{\partial y} = 0, \tag{13}$$

$$S_{xx} - 2\lambda_1\ S_{xy}\frac{\partial u}{\partial y} = 0, \tag{14}$$

$$S_{xy}\ or\ S_{yx} - \lambda_1\ S_{yy}\frac{\partial u}{\partial y} = \frac{\mu_{nf}}{\mu_f}\frac{\partial u}{\partial y}, \tag{15}$$

$$S_{yy} = 0, \tag{16}$$

After eliminating the pressure between Eqs. (11) and (12) and using (16), the equations of motion in terms of the stream function ψ $\left(\text{where } u = \frac{\partial\psi}{\partial y}, v = -\frac{\partial\psi}{\partial x}\right)$, will be

$$\psi_{yyyy} - \Gamma^2\psi_{yy} + G_r\frac{(\rho\alpha)^*}{\mu^*}\ \Theta_y = 0, \tag{17}$$

$$\Theta_{yy} + B_r\frac{\mu^*}{k^*}\left(\psi_{yy}\right)^2 = 0, \tag{18}$$

Table 1 The values of thermo-physical properties of some base fluids and nanoparticles

Base Fluid (UCM)	ρ_f(kg/m^3)	k_f(W/m. K)	α_f(K^{-1})	σ_f(Ω^{-1}. m^{-1})
Pure Water	997.1	0.613	2.10E-04	0.05
Ethylene Glycol	1114	0.252	6.50E-04	1.07
Blood	1060	0.542	1.00E-04	0.7
Nanoparticles	**ρ_p(kg/m^3)**	**k_p(W/m. K)**	**α_p(K^{-1})**	**σ_p(Ω^{-1}. m^{-1})**
Copper (Cu)	8933	401	1.67E-05	5.96E+07
Silver (Ag)	10500	429	1.89E-05	6.30E+07
Gold (Au)	19300	318	1.42E-05	4.52E+07
Alumina (Al_2O_3)	3970	40	8.50E-06	1.50E-07
Titanium Oxide (TiO_2)	4250	8.9538	9.00E-06	1.00E-12

where $\Gamma^2 = \left(\frac{\sigma^*}{\mu^*}M^2 + \frac{1}{K}\right)$, $P_r E_c = B_r$ is the Brinkman number, the dynamic viscosity of nanofluids Sheikholeslami *et al.* (2012) is

$$\mu^* = \frac{\mu_{nf}}{\mu_f} = \frac{1}{(1-\phi)^{2.5}}, \tag{19}$$

the relation of effective density and thermal expansion coefficient of the nanofluid is

$$(\rho\alpha)^* = \frac{(\rho\alpha)_{nf}}{(\rho\alpha)_f} = 1 + \phi\ [(\rho\alpha)_r - 1], \tag{20}$$

the effective thermal conductivity of the nanofluid according to Hamilton and Crosser (1962) is

$$k^* = \frac{k_{nf}}{k_f} = 1 + \frac{\phi\, m\, [k_r - 1]}{m + (1-\phi)[k_r - 1]}, \tag{21}$$

the effective electrical conductivity of nanofluid was presented by Sheikholeslami *et al.* (2014) as

$$\sigma^* = \frac{\sigma_{nf}}{\sigma_f} = 1 + \frac{3\phi[\sigma_r - 1]}{3 + (1-\phi)\ [\sigma_r - 1]}, \tag{22}$$

with

$$(\rho\alpha)_r = \frac{(\rho\alpha)_p}{(\rho\alpha)_f}, \qquad k_r = \frac{k_p}{k_f}, \qquad \sigma_r = \frac{\sigma_p}{\sigma_f},$$

where $(.)_p$ is the physical property for nanoparticles and $(.)_r$ is the ratio of the same property. ϕ is the nanoparticle volume fraction ($\phi = 0.05$ through the paper), m is the shape factor, $m = \frac{3}{\xi}$, ξ is the sphericity which is used to characterize shape for particle falling through fluids. Table 1 refers to the values of thermo-physical properties of some base fluids and nanoparticles at temperature 300 K, (Sheikholeslami and Ganji 2017, Sobamowo 2018 and, Turns and Kraige 2007). Table (2) refers to the calculated values of effective ratios of thermophysical properties of previous base fluids and nanoparticles.

Then the appropriate dimensionless boundary conditions in terms of the stream function are

Table 2 The values of effective ratios of thermo-physical properties of previous base fluids and nanoparticles

Nanoparticles	Base Fluid (UCM)								
	Pure Water			Ethylene Glycol			Blood		
	$(\rho\alpha)_r$	k_r	σ_r	$(\rho\alpha)_r$	k_r	σ_r	$(\rho\alpha)_r$	k_r	σ_r
Copper (Cu)	0.7125	654	1.19E+09	0.2060	1591	5.57E+07	1.4074	740	8.51E+07
Silver (Ag)	0.9478	700	1.26E+09	0.2740	1702	5.89E+07	1.8722	792	9.00E+07
Gold (Au)	1.3088	519	9.04E+08	0.3785	1261	4.22E+07	2.5855	587	6.46E+07
Alumina (Al_2O_3)	0.1612	65	3.00E-06	0.0466	159	1.40E-07	0.3183	74	2.14E-07
Titanium Oxide (TiO_2)	0.1827	15	2.00E-11	0.0528	36	0.35E-13	0.3608	17	1.43E-12

$$\psi = \frac{q}{2}, \qquad \psi_y = -1, \quad \Theta = 0, \quad at \quad y = h = 1 + b\sin 2\pi x, \tag{23}$$

$$\psi = -\frac{q}{2}, \qquad \psi_y = -1, \quad \Theta = 1, \quad at \quad y = -h = -1 - b\sin 2\pi x \tag{24}$$

where q represents fluid flow rate in wave frame and will discuss in details in pumping characteristics.

3. Solution procedure

The governing differential Eqs. (17) and (18) with boundary conditions (23,24) consist of non-linear and coupled equations. Getting the exact solution of the governing system of equations is difficult and unavailable. Therefore, using the perturbation method may give an analytical solution to the system. By taking Brinkman number B_r as a perturbation parameter, we expand the functions $\psi(x,y)$ and $\Theta(x,y)$ as follows

$$\psi(x,y) = \psi_0(x,y) + B_r\ \psi_1(x,y) + B_r^2\ \psi_2(x,y) + \ldots$$

$$\Theta(x,y) = \Theta_0(x,y) + B_r\ \Theta_1(x,y) + B_r^2\ \Theta_2(x,y) + \ldots$$

Substituting into the differential Eqs. (17) and (18) and boundary conditions (23) and (24), we have

3.1 Zero order

$$(\psi_0)_{yyyy} - \Gamma^2(\psi_0)_{yy} + G_r\frac{(\rho\alpha)^*}{\mu^*}\ (\Theta_0)_y = 0, \tag{25}$$

$$(\Theta_0)_{yy} = 0, \tag{26}$$

$$\psi_0 = \frac{q}{2}, \qquad (\psi_0)_y = -1, \quad \Theta_0 = 0, \quad at \quad y = h = 1 + b\sin 2\pi x, \tag{27}$$

$$\psi_0 = -\frac{q}{2}, \qquad (\psi_0)_y = -1, \quad \Theta_0 = 1, \quad at \quad y = -h = -1 - b\sin 2\pi x \tag{28}$$

The exact solution of zero order stream and heat functions are given as

$$\psi_0(x,y) = -y + (q+2h)\left[\frac{\sinh(\Gamma y) - \Gamma y\cosh(\Gamma h)}{2\sinh(\Gamma h) - 2h\Gamma\cosh(\Gamma h)}\right] + G_r\frac{(\rho\alpha)^*}{\mu^*}\left[\frac{(h^2-y^2)}{4\Gamma^2 h} + \frac{\cosh(\Gamma y) - \cosh(\Gamma h)}{2\Gamma^3\sinh(\Gamma h)}\right] \tag{29}$$

$$\Theta_0(x,y) = \frac{h-y}{2h} \tag{30}$$

3.2 First order

$$(\psi_1)_{yyyy} - \Gamma^2(\psi_1)_{yy} + G_r\frac{(\rho\alpha)^*}{\mu^*}\ (\Theta_1)_y = 0, \tag{31}$$

$$(\Theta_1)_{yy} + \frac{\mu^*}{k^*}\left((\psi_0)_{yy}\right)^2 = 0, \tag{32}$$

$$\psi_1 = 0, \ (\psi_1)_y = 0, \ \Theta_1 = 0, \quad at \quad y = h = 1 + b\sin 2\pi x, \tag{33}$$

$$\psi_1 = 0, \ (\psi_1)_y = 0, \ \Theta_1 = 0, \quad at \quad y = -h = -1 - b\sin 2\pi x \tag{34}$$

$$\psi_1(x,y) = L_1 + L_2 y + L_3\sinh(\Gamma y) + L_4\cosh(\Gamma y) + G_r\frac{(\rho\alpha)^*}{6\mu^*\Gamma^3}[C_4\sinh(2\Gamma y) + C_3\cosh(2\Gamma y) + 3\Gamma C_1 y\sinh(\Gamma y) + 3\Gamma C_2 y\cosh(\Gamma y) + (h^2-y^2)(2\Gamma C_5 y - 3\Gamma C_6)], \tag{35}$$

$$\Theta_1(x,y) = -C_1\sinh(\Gamma y) - C_2\cosh(\Gamma y) - C_3\sinh(2\Gamma y) - C_4\cosh(2\Gamma y) - C_5 y^2 + C_6 y + C_7 \tag{36}$$

where

$$C_1 = G_r\frac{(\rho\alpha)^*}{2k^*\Gamma^2 h}\left[\frac{(q+2h)}{\Gamma h\cosh(\Gamma h) - \sinh(\Gamma h)}\right],$$

$$C_2 = -G_r^2\frac{(\rho\alpha)^{*2}}{2\mu^* k^*\Gamma^5 h}\left[\frac{1}{\sinh(\Gamma h)}\right],$$

$$C_3 = -G_r\frac{(\rho\alpha)^*}{8k^*\Gamma}\left[\frac{(q+2h)}{1 - \cosh(2\Gamma h) + \Gamma h\sinh(2\Gamma h)}\right],$$

$$C_4=\frac{C_3}{2}\left[\frac{C_2}{C_1}+\frac{C_1}{C_2}\right], C_5=\Gamma^2\left[\frac{C_2C_3}{C_1}-\frac{C_1C_3}{C_2}+\frac{C_1C_2}{32C_3}\right],$$

$$C_6=\frac{1}{h}[C_1\sinh(\Gamma h)+C_3\sinh(2\Gamma h)],$$

$$C_7=C_2\cosh(\Gamma h)+C_4\cosh(2\Gamma h)+C_5h^2,$$

$$L_1=G_r\frac{(\rho\alpha)^*}{4\mu^*\Gamma^3}\left[C_3+\frac{\begin{matrix}6\Gamma hC_1+12hC_6\cosh(\Gamma h)\\+3C_1\sinh(2\Gamma h)+C_3\sinh(3\Gamma h)\end{matrix}}{3\sinh(\Gamma h)}\right],$$

$$L_2=G_r\frac{(\rho\alpha)^*}{12\mu^*\Gamma^2}\left[\frac{\begin{matrix}-6\Gamma hC_2-(3C_4+8h^2C_5)\sinh(\Gamma h)\\+3C_2\sinh(2\Gamma h)+C_4\sinh(3\Gamma h)\end{matrix}}{\Gamma h\cosh(\Gamma h)-\sinh(\Gamma h)}\right],$$

$$L_3=G_r\frac{(\rho\alpha)^*}{6\mu^*\Gamma^3}\left[\frac{\begin{matrix}4\Gamma h^3C_5-3\Gamma^2h^2C_2\sinh(\Gamma h)\\+C_4\sinh(2\Gamma h)-2\Gamma hC_4\cosh(2\Gamma h)\end{matrix}}{\Gamma h\cosh(\Gamma h)-\sinh(\Gamma h)}\right],$$

$$L_4=-G_r\frac{(\rho\alpha)^*}{6\mu^*\Gamma^3}\left[3C_1+\frac{\begin{matrix}6hC_6+3\Gamma hC_1\cosh(\Gamma h)\\+2C_3\sinh(2\Gamma h)\end{matrix}}{\sinh(\Gamma h)}\right]$$

4. Pumping characteristics

The rate of fluid flow in the wave frame can be expressed as:

$$q=\int_{-h}^{h}u(x,y,t)dy \tag{37}$$

While the fluid flow rate in the laboratory frame can be written as

$$Q=\int_{-H}^{H}U(X,Y,t)dY \tag{38}$$

From the equations that used to convert from the laboratory frame to the wave frame, $X=x+t$ and $U=u+1$ we can conclude the following relationship

$$Q=q+2h \tag{39}$$

Supposing we are dealing with a device of a pumping nature, accordingly, it is good to find a discharge rate $\bar{Q}$, which can be used as the meantime of the volumetric flow rate for each cross-section as

$$\frac{dp(x)}{dx}=\frac{dp_0(x)}{dx}+B_r\frac{dp_1(x)}{dx}+\ldots \tag{40}$$

where

$$\frac{dp_0(x)}{dx}=\frac{\rho\alpha G_r}{2}-\frac{\mu\Gamma^3(q+2h)\cosh(\Gamma h)}{2h\Gamma\cosh(\Gamma h)-2\sinh(\Gamma h)}$$

$$\frac{dp_1(x)}{dx}=\rho\alpha G_rC_7-\mu\Gamma^2L_2-\frac{\rho\alpha G_r(6-\Gamma^2h^2)}{3\Gamma^2}C_5$$

By integrating the axial pressure gradient (40) over one wavelength λ, the pressure rise is given by

$$\begin{aligned}\Delta p&=\int_0^1\frac{dp}{dx}\,dx=\int_0^1\left(\frac{dp_0}{dx}+B_r\frac{dp_1}{dx}+\cdots\right)dx\\&=\Delta p_0+B_r\Delta p_1+\ldots\end{aligned} \tag{41}$$

where

$$\Delta p_0=\frac{\rho\alpha G_r}{2}-\int_0^1\frac{\mu\Gamma^3(\bar{Q}-2+2h)\cosh(\Gamma h)}{2h\Gamma\cosh(\Gamma h)-2\sinh(\Gamma h)}dx$$

$$\Delta p_1=\int_0^1\left(\rho\alpha G_rC_7-\mu\Gamma^2L_2-\frac{\rho\alpha G_r(6-\Gamma^2h^2)}{3\Gamma^2}C_5\right)dx$$

5. Results and discussion

In this section, we deal with the effects of different parameters as: Hartmann number, M, Grashof number G_r, permeability parameter K, nanoparticle sphericity ξ, thermal expansion ratio $(\rho\alpha)_r$, thermal conductivity ratio k_r and electrical conductivity ratio σ_r (the values of last three parameters are computed as Table 2) on the pressure rise Δp pressure gradient $\partial p/\partial x$, vertical velocity distribution u, heat function distribution Θ and trapping phenomenon.

5.1 Pumping performance and pressure gradient

Figs. 2(a)-2(e) illustrate the effect of some parameters on the variation of the pressure rise with the volume flow rate (pumping performance) at a particular value of Δp. In Fig. 2(a) it is seen that pressure rise is directly proportional to (G_r) in all pumping regions therefore, pumping performance improves with increasing (G_r) our results completely agree with Sayed *et al*. (2016).

In Fig. 2(b) we notice that pressure rise is inversely proportional to (K) in the peristaltic pumping region $(\Delta p>0)$ and at free pumping $(\Delta p=0)$ the flux increased with increasing (K). In contrast, pressure rise is directly proportional to (K) in the augmented peristaltic pumping region $(\Delta p<0)$. As shown in Fig. 2(c) we notice the contrariwise effect of M. Fig. 2(d) explains the effect of the nanoparticle shape ξ, it is observed the pumping is improved where $\bar{Q}$ increased with ξ. Also, in Fig. 2(e) there is an improvement of the pumping because of the effect of thermal expansion ratio $(\rho\alpha)_r$ where $\bar{Q}$ increasing with it.

Figs. 3(a)-3(f) illustrate some parameters on the variation of the pressure gradient with x. From Fig. 3(a) it is observed that $\partial p/\partial x$ increasing with $\bar{Q}$ through the fluid motion. In the contraction region, the variation is higher than it in the expansion region. Fig. 3(b) explained that $\partial p/\partial x$ increasing with the effect of G_r. Looking at Fig. 3(c) we get that in the expansion region $\partial p/\partial x$ increasing with K and in the contraction region (confined between two values at which there is no variation) $\partial p/\partial x$ decreasing with K, in Fig. 3(d) we notice the contrariwise for the effect of M on $\partial p/\partial x$. In Figs. 3(e) and 3(f) it is clear that $\partial p/\partial x$ increasing with ξ and $(\rho\alpha)_r$ but in Fig. 3(e) the variation increasing as ξ decreasing and in Fig. 3(f) the variation increasing with $(\rho\alpha)_r$.

Figs. 4(a)-4(d) explained some parameters on the relation between the heat function Θ and y at different values of x (the value of x just indicates the position of the plot in peristaltic wave and the real axes of each plot are (y,Θ), the range of y is the base of shaded triangle

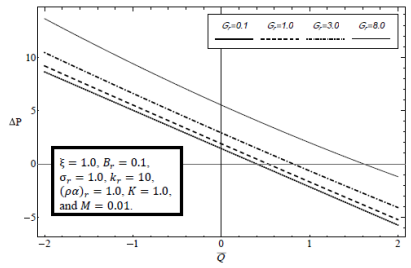

(a) Effect of Grashof number G_r

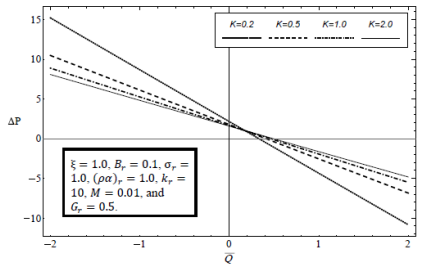

(b) Effect of permeability K

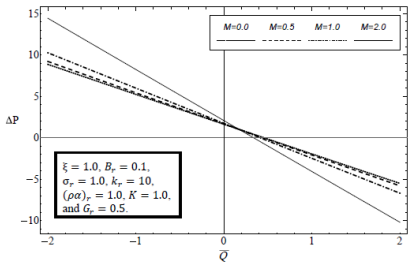

(c) Effect of magnetic parameter M

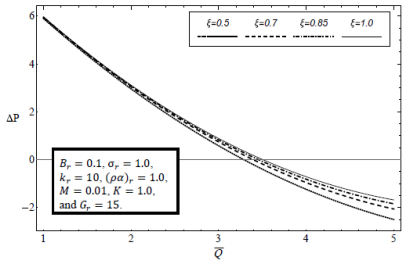

(d) Effect of nanoparticle shape parameter ξ

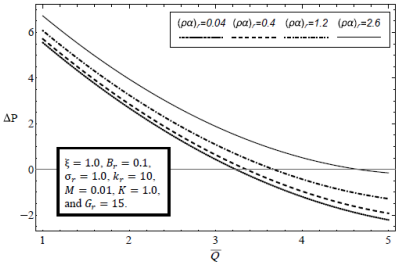

(e) Effect of thermal expansion ratio $(\rho\alpha)_r$

Fig. 2 The pressure rise ΔP versus volume flow rate $\bar{Q}$

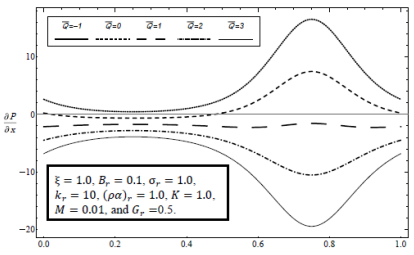

(a) Effect of Volume flow rate $\bar{Q}$

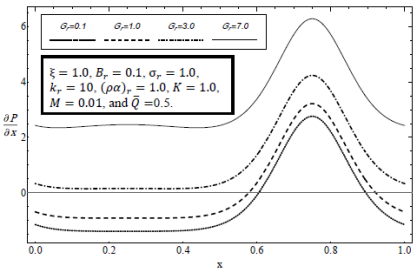

(b) Effect of Grashof number G_r

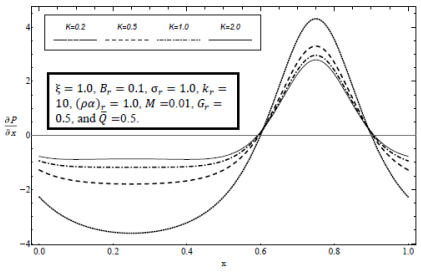

(c) Effect of permeability K

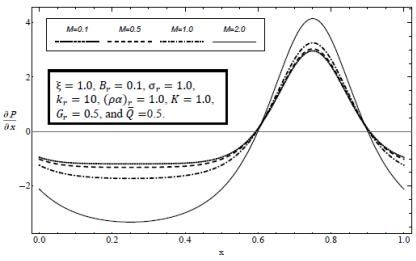

(d) Effect of magnetic parameter M

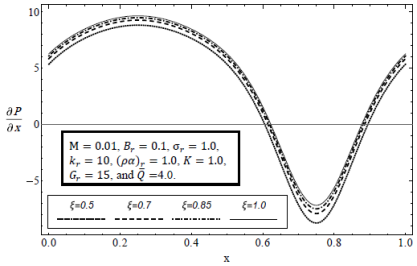

(e) Effect of nanoparticle shape parameter ξ

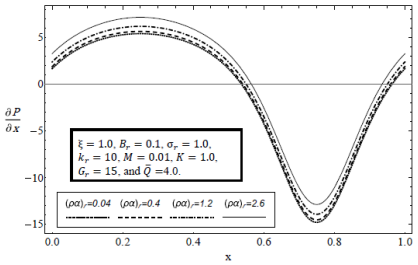

(f) Effect of thermal expansion ratio $(\rho\alpha)_r$

Fig. 3 The pressure gradient $\partial P/\partial x$ versus x

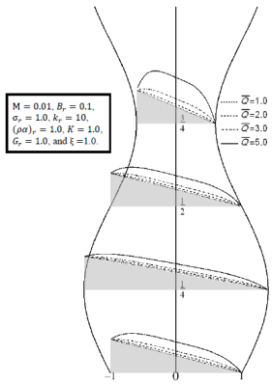

(a) Effect of volume flow rate $\bar{Q}$

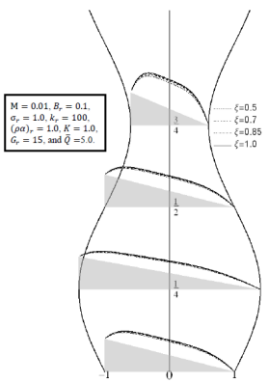

(b) Effect of nanoparticle shape parameter ξ

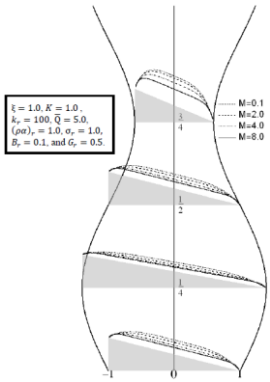

(c) Effect of magnetic parameter M

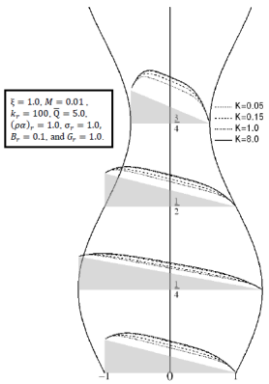

(d) Effect of permeability K

Fig. 4 Heat function versus y through the channel at $x = 0, \frac{1}{4}, \frac{1}{2}, \frac{3}{4}$

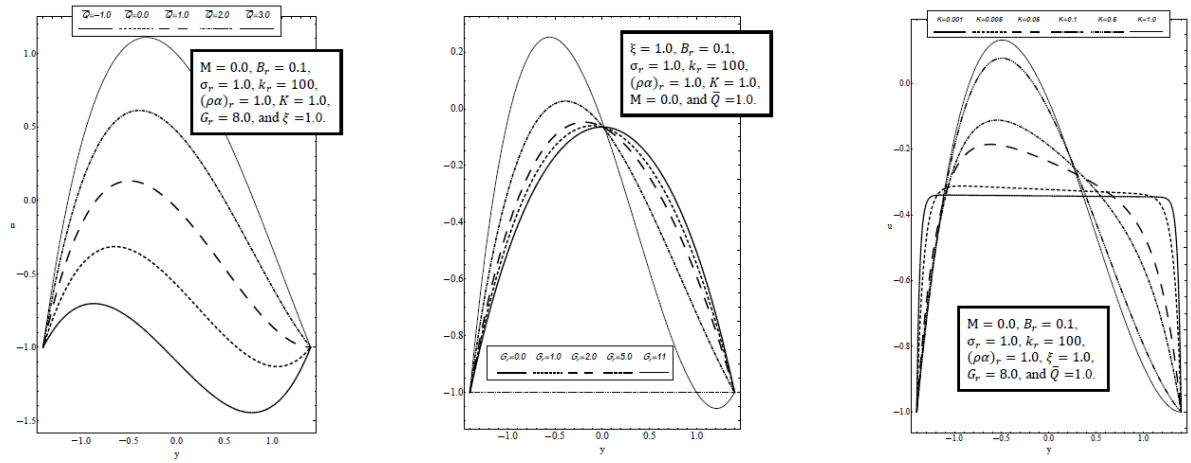

(a) Effect of Volume flow rate $\bar{Q}$ (b) Effect of Grashof number G_r (c) Effect of permeability K

(d) Effect of magnetic parameter M (e) Effect of thermal expansion ratio $(\rho\alpha)_r$

Fig. 5 The vertical velocity function u versus y

$[-h, h]$ and the value of Θ is depends on the boundary conditions $\Theta(-h) = 1, \Theta(h) = 0$).). In Fig. 4(a) it is observed that the temperature Θ increases with $\bar{Q}$. The temperature increases with ξ but with a weak effect, which is explained in Fig. 4(b). In Fig. 4(c) Θ is decreasing with an increase of M and the contrariwise for the effect of K on Θ is observed in Fig. 4(d).

5.2 The vertical velocity

Figs. 5(a)-5(e) explained the effect of some physical parameters on the relation between the vertical velocity function and y. Considering that the system is an isothermal where the cold wall at $y = h$ and the hot wall at $y = -h$, in Fig. (5a) we noticed that the velocity increased with $\bar{Q}$ and the velocity near the hot is more than it near the cold wall. In Fig. 5(b) there are two regions, one from the hot wall to the center of the channel in which u increased with G_r. The second one is from the center of the channel to the cold wall, in which it is observed u decreased with G_r and this results match with Cheng *et al*. (1990) .

In Fig. 5(c) the effect of the permeability parameter K is studied, at small values of K (K=0.001 and K=0.005) it is clear that u is constant (there is no effect of the heat on the velocity) after we chose big values of K(0.05 to 1.0) we had two regions one near the hot wall in which u increased with K and the other near the cold wall in which u decreased with K.

Fig. 5(d) is plotted to explain the effect of the magnetic parameter M which has the vice verse effect of K, also, the effect of both K and M are discussed by Prakash *et al*. (2019). The Effect of thermal expansion ratio $(\rho\alpha)_r$ on vertical velocity u is illustrated in Fig. 5(e) where u increased with $(\rho\alpha)_r$ near the hot wall and u decreased with $(\rho\alpha)_r$ near the cold wall.

5.3 Trapping phenomenon

The phenomenon of trapping is considered when studying peristaltic motion and the effect of various parameters on it is studied. In this paper, there is a change in the temperature of the channel walls, the velocity of the fluid particles near the hot wall increased as noted in the discussion of vertical velocity.

Consider Fig. 6(a), which plots the contours of stream function versus its local position (x, y) with no heat effect $G_r = 0$, the right and left bolus are similar. By increasing

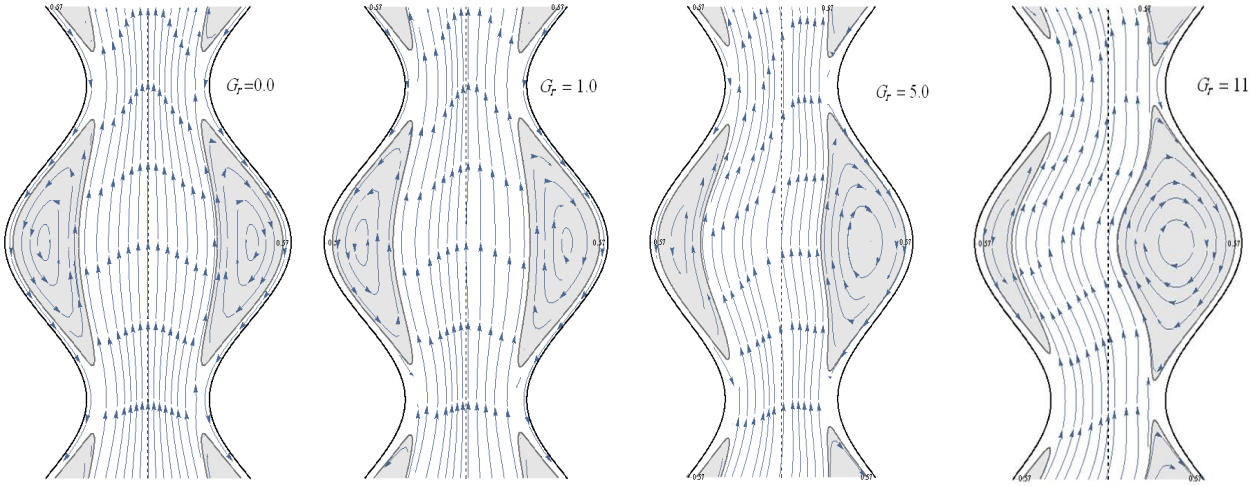

(a) (b) (c) (d)

Fig. 6 Contour plot of stream function with $\xi = 1.0,\ B_r = 0.1,\ \sigma_r = 1.0,\ k_r = 100,\ M = 0, K = 1.0,\ \bar{Q} = 3.0$ and $(\rho\alpha)_r = 1.0$

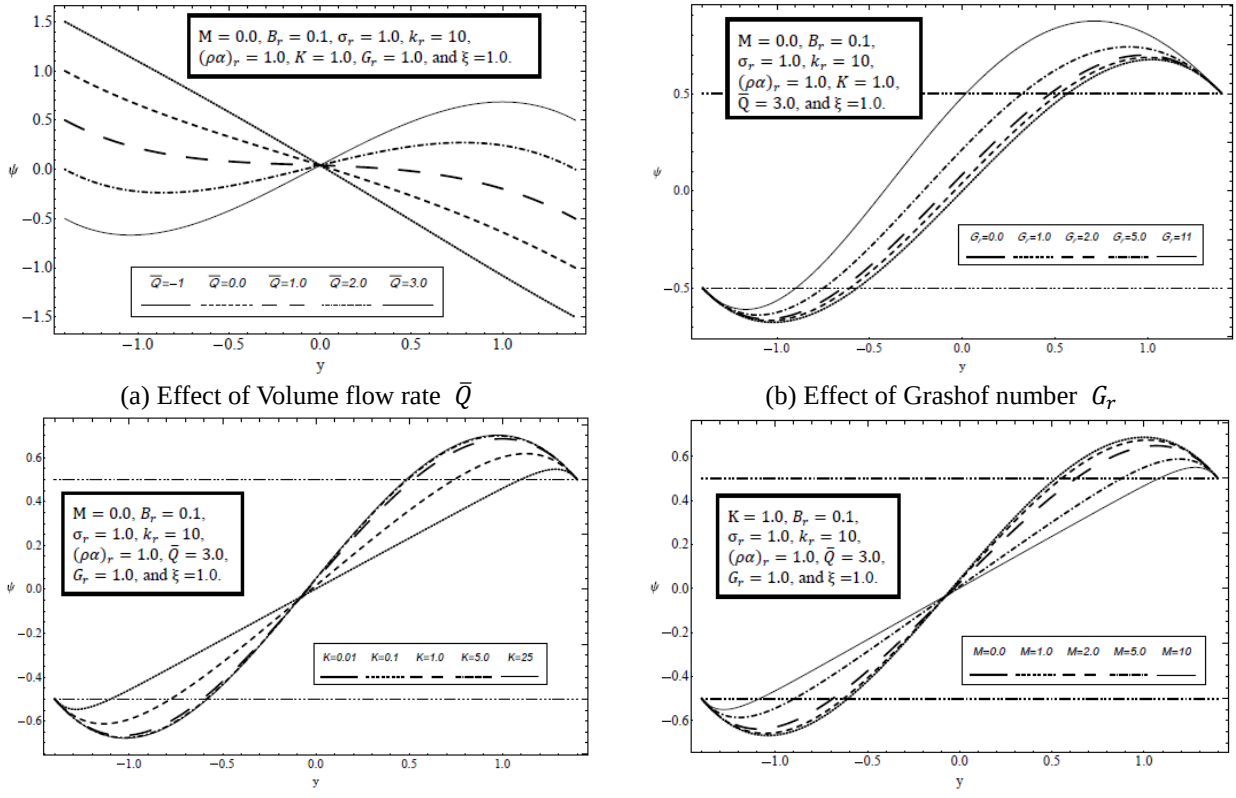

(a) Effect of Volume flow rate $\bar{Q}$

(b) Effect of Grashof number G_r

(c) Effect of permeability K

(d) Effect of magnetic parameter M

Fig. 7 The stream function versus y at $x = 0.25$

G_r the size of the right increased while the size of the left decreased, as seen in Figs. 6(b)-6(d), respectively.

To explain that, our problem is considered with isothermal walls (the temperature is constant at each wall) and G_r is considered as a buoyancy parameter. In their study, Boulama and Galanis [30] indicate that by increasing the buoyancy parameter G_r, the particles near the hot wall accelerate while the particles near the cooler wall decelerate and sometimes reverse thier sign. From the above we can explain why the bolus enlarges at the cooler wall and diminishes at the hot wall.

In the case of a symmetrical channel, instead of using four figures of the trapping phenomenon (Figs. 6(a)-6(d)) to discuss the effect of one parameter (G_r), the authors suggested a new technique by using a single curve for the stream function. This curve represents the stream function curve at the center of the swollen area $\psi\left(\frac{1}{4}, y\right)$ versus y. By plotting two horizontal lines at

$$\psi = \pm\frac{q}{2} = \pm\left(\frac{\bar{Q}}{2} - 1\right),$$

The trapping occurred when the horizontal lines intersect the curve in two points and the distance between these points represents the size of the bolus.

Fig. 7(a) shows the effect of the volume flow rate on the trapping phenomenon's appearance. It is clear that at a specific $\bar{Q}$ value, the bolus starts to appear on the line of symmetry. With increasing $\bar{Q}$, the bolus takes place towards the walls, as shown in the figure with $\bar{Q} = 2{,}3$.

Fig. 7(b) explained the effect of G_r on the trapping and it is observed that the bouls of trapping near the hot wall are smaller than it near the cold for each value of G_r. In Fig. 7(c) we observed that near the walls, the trapping bouls increased with K and there is no trapping near the center of the channel, from Fig. 7(d) it is clear that the trapping bulse is decreased with M.

6. Conclusions

A detailed analysis of the peristaltic transport of nanofluid in a symmetric heated vertical channel is presented. The pumping characteristics, heat function, flow velocity and trapping phenomena are analyzed for various parameter values of upper convected Maxwell fluid. Based on the graphs and the solution, it can be concluded that:

• The pumping performance improves in the augmented peristaltic pumping region with the increase of G_r , K, ξ and $(\rho\alpha)_r$ and the decrease of M.

• In the relation between the pressure gradient and x, all parameters' effect is clear at the center of the contraction region.

• There is no remarkable effect for thermal conductivity ratio k_r and electrical conductivity ratio σ_r on the pressure gradient.

• In heat function distribution, the minimum values of Θ at the center of the expansion region and the maximum values at the center of the contraction region.

• The flow velocity near the hot wall increases and decreases near the cold wall and sometimes reverses.

• Grashof number has a clear effect on the volume of trapping bolus.

• There is no remarkable effect for the nanoparticle shape ξ, thermal conductivity ratio k_r and electrical conductivity ratio σ_r on the velocity and trapping.

References

Abbasi, F.M., Hayat, T. and Ahmad, B. (2015), "Peristaltic transport of copper–water nanofluid saturating porous medium", *Physica E*, **67**, 47-53. https://doi.org/10.1016/j.physe.2014.11.002.

Abd Elmaboud, Y. (2018), "Two layers of immiscible fluids in a vertical semi-corrugated channel with heat transfer: Impact of nanoparticles", *Results Phys*., **9**, 1643-1655. https://doi.org/10.1016/j.rinp.2018.05.008.

Akbar, N.S., Butt, A.W. and Tripathi, D. (2017), "Nanoparticle shapes effects on unsteady physiological transport of nanofluids through a finite length non-uniform channel", *Results Phys*., **7**, 2477-2484. https://doi.org/10.1016/j.rinp.2017.07.019.

Akbar, N.S., Nadeem, S., Hayat, T. and Hendi, A.A. (2012), "Peristaltic flow of a nanofluid in a non-uniform tube", *Heat Mass Transf*., **48**(3), 451-459. https://doi.org/10.1007/s00231-011-0892-7.

Amin, M.T. and Alazba, A.A. (2014), "A review of nanomaterials based membranes for removal of contaminants from polluted waters", *Membr. Water Treat*., **5**(2), 123-146 https://doi.org/10.12989/mwt.2014.5.2.123.

Boulama, K. and Galanis, N. (2004), "Analytical solution for fully developed mixed convection between parallel vertical plates with heat and mass transfer", *J. Heat Transfer*, **126**(3), 381-388. https://doi.org/10.1115/1.1737774.

Buschmann, M.H. and Franzke, U. (2014), "Improvement of thermosyphon performance by employing nanofluid", *Int. J. Refrig*., **40**, 416-428. https://doi.org/10.1016/j.ijrefrig.2013.11.022.

Chen, T., Kim, J. and Cho, H. (2014), "Theoretical analysis of the thermal performance of a plate heat exchanger at various chevron angles using lithium bromide solution with nanofluid", *Int. J. Refrig*., **48**, 233-244. https://doi.org/10.1016/j.ijrefrig.2014.08.013.

Cheng, C.H., Kou, H. Sen and Huang, W.H. (1990), "Flow reversal and heat transfer of fully developed mixed convection in vertical channels", *J. Thermophys. Heat Transf*., **4**(3), 375-383. https://doi.org/10.2514/3.190.

Elmaboud, Y.A., Mekheimer, K.S. and Emam, T.G. (2019), "Numerical examination of gold nanoparticles as a drug carrier on peristaltic blood flow through physiological vessels: Cancer therapy treatment", *Bionanoscience*, **9**(4), 952-965. https://doi.org/10.1007/s12668-019-00639-7.

Ghasemi, S.E., Vatani, M., Hatami, M. and Ganji, D.D. (2016), "Analytical and numerical investigation of nanoparticle effect on peristaltic fluid flow in drug delivery systems", *J. Mol. Liq*., **215**, 88-97. https://doi.org/10.1016/j.molliq.2015.12.001.

Hamilton, R.L. and, Crosser, O.K. (1962), "Thermal conductivity of heterogeneous two-component systems", *Ind. Eng. Chem. Fundam*., **1**(3), 187-191. https://doi.org/10.1021/i160003a005.

Hayat, T., Aslam, N., Alsaedi, A. and Rafiq, M. (2017), "Numerical study for MHD peristaltic transport of Sisko nanofluid in a curved channel", *Int. J. Heat Mass Transf*., **109**, 1281-1288. https://doi.org/10.1016/j.ijheatmasstransfer.2017.01.121.

Hayat, T., Nisar, Z., Yasmin, H. and Alsaedi, A. (2016), "Peristaltic transport of nanofluid in a compliant wall channel with convective conditions and thermal radiation", *J. Mol. Liq*., **220**, 448-453. https://doi.org/10.1016/j.molliq.2016.04.080.

Ibrahim, M.G., Hasona, W.M. and ElShekhipy, A.A. (2019), "Concentration-dependent viscosity and thermal radiation effects on MHD peristaltic motion of synovial nanofluid: Applications to rheumatoid arthritis treatment", *Comput. Methods Programs Biomed*., **170**, 39-52. https://doi.org/10.1016/j.cmpb.2019.01.001.

Kot, M.A.E.L. and Elmaboud, Y.A.B.D. (2021), "Hybrid nanofluid flows through a vertical diseased coronary artery with heat transfer", *J. Mech. Med. Biol*., **21**(2). https://doi.org/10.1142/S0219519421500123.

Mohamad, R.B., Kandasamy, R. and Muhaimin, I. (2013), "Enhance of heat transfer on unsteady Hiemenz flow of nanofluid over a porous wedge with heat source/sink due to solar energy radiation with variable stream condition", *Heat Mass Transf*., **49**(9), 1261-1269. https://doi.org/10.1007/s00231-013-1163-6.

Mosayebidorcheh, S. and Hatami, M. (2018), "Analytical investigation of peristaltic nanofluid flow and heat transfer in an asymmetric wavy wall channel (Part I: Straight channel)", *Int. J. Heat Mass Transf*., **126**, 790-799.

https://doi.org/10.1016/j.ijheatmasstransfer.2018.05.080.
Noreen, S. (2018), "Peristaltically assisted nanofluid transport in an asymmetric channel", *Karbala Int. J. Mod. Sci.*, **4**(1), 35-49. https://doi.org/10.1016/j.kijoms.2017.10.005.
Prakash, J., Siva, E.P., Tripathi, D., Kuharat, S. and Bég, O.A. (2019), "Peristaltic pumping of magnetic nanofluids with thermal radiation and temperature-dependent viscosity effects: Modelling a solar magneto-biomimetic nanopump", *Renew. Energy*, **133**, 1308-1326. https://doi.org/10.1016/j.renene.2018.08.096.
Rachid, H. (2015), "Effects of heat transfer and an endoscope on peristaltic flow of a fractional maxwell fluid in a vertical tube", *Abstr. Appl. Anal.*, 360918. https://doi.org/10.1155/2015/360918.
Reddy, M.G. and Makinde, O.D. (2016), "Magnetohydrodynamic peristaltic transport of Jeffrey nanofluid in an asymmetric channel", *J. Mol. Liq.*, **223**, 1242-1248. https://doi.org/10.1016/j.molliq.2016.09.080.
Sadaf, H., Akbar, M.U. and Nadeem, S. (2018), "Induced magnetic field analysis for the peristaltic transport of non-Newtonian nanofluid in an annulus", *Math. Comput. Simul.*, **148**, 16-36. https://doi.org/10.1016/j.matcom.2017.12.009.
Sayed, H.M., Aly, E.H. and Vajravelu, K. (2016), "Influence of slip and convective boundary conditions on peristaltic transport of non-Newtonian nanofluids in an inclined asymmetric channel", *Alexandria Eng. J.*, **55**(3), 2209-2220. https://doi.org/10.1016/j.aej.2016.04.041.
Shah, N.A., Animasaun, I.L., Ibraheem, R.O., Babatunde, H.A., Sandeep, N. and Pop, I. (2018), "Scrutinization of the effects of Grashof number on the flow of different fluids driven by convection over various surfaces", *J. Mol. Liq.*, **249**, 980-990. https://doi.org/10.1016/j.molliq.2017.11.042.
Sharif, H., Khadimallah, M.A., Naeem, M.N., Hussain, M., Hussain, S. and Tounsi, A. (2021), "Flow of MHD Powell-Eyring nanofluid: Heat absorption and Cattaneo-Christov heat flux model", *Adv. Nano Res.*, **10**(3), 221-234. https://doi.org/10.12989/anr.2021.10.3.221.
Sheikholeslami, M., Gorji-Bandpy, M., Ganji, D.D., Soleimani, S. and Seyyedi, S.M. (2012), "Natural convection of nanofluids in an enclosure between a circular and a sinusoidal cylinder in the presence of magnetic field", *Int. Commun. Heat Mass Transf.*, **39**(9), 1435-1443. https://doi.org/10.1016/j.icheatmasstransfer.2012.07.026.
Sheikholeslami, M., Gorji-Bandpy, M., Ganji, D.D. and Soleimani, S. (2014), "Heat flux boundary condition for nanofluid filled enclosure in presence of magnetic field", *J. Mol. Liq.*, **193**, 174-184. https://doi.org/10.1016/j.molliq.2013.12.023.
Sheikholeslami, M. and Ganji, D.D. (2017), *Applications of Nanofluid for Heat Transfer Enhancement*, Elsevier Inc, New York, U.S.A.
Sobamowo, M. (2018), "Slip analysis of magnetohydrodynamics flow of an upper-convected Maxwell viscoelastic nanofluid in a permeable channel embedded in a porous medium", *Aeronaut. Aerosp. Open Access J.*, **2**(5). https://doi.org/10.15406/aaoaj.2018.02.00065.
Sözen, A., Özbaş, E., Menlik, T., Çakir, M.T., Gürü, M. and Boran, K. (2014), "Improving the thermal performance of diffusion absorption refrigeration system with alumina nanofluids: An experimental study", *Int. J. Refrig.*, **44**, 73-80. https://doi.org/10.1016/j.ijrefrig.2014.04.018.
Timofeeva, E.V., Routbort, J.L. and Singh, D. (2009), "Particle shape effects on thermophysical properties of alumina nanofluids", *J. Appl. Phys.*, **106**(1), 014304. https://doi.org/10.1063/1.3155999.
Turns, S. and Kraige, D. (2007), *Property Tables for Thermal Fluids Engineering*, Cambridge University Press, Campridge, U.K.
Vajravelu, K., Sreenadh, S. and Lakshminarayana, P. (2011), "The influence of heat transfer on peristaltic transport of a Jeffrey fluid in a vertical porous stratum", *Commun. Nonlinear Sci. Numer. Simul.*, **16**(8), 3107-3125. https://doi.org/10.1016/j.cnsns.2010.11.001.

CC